SCIENCE CHINA
Physics, Mechanics & Astronomy

• Invited Review •

July 2017 Vol. 60 No. 7: 074201
doi: 10.1007/s11433-017-9035-8

Perspective on how laser-ablated particles grow in liquids

DongShi Zhang*, Jun Liu, and ChangHao Liang*

Key Laboratory of Materials Physics and Anhui Key Laboratory of Nanomaterials and Nanotechnology, Institute of Solid State Physics, Chinese Academy of Sciences, Hefei 230031, China

Received March 11, 2017; accepted April 7, 2017; published online May 12, 2017

Laser ablation in liquids has emerged as a new branch of nanoscience for developing various nanomaterials with different shapes. However, how to design and control nanomaterial growth is still a challenge due to the unique chemical-physical process chain correlated with nanomaterial nucleation and growth, including plasma phase (generation and rapid quenching), gas (bubble) phase, and liquid phase. In this review, through summarizing the literature about this topic and comparing with the well-established particle growth mechanisms of the conventional wet chemistry technique, our perspective on the possible nanoparticle growth mechanisms or routes is presented, aiming at shedding light on how laser-ablated particles grow in liquids. From the microscopic viewpoint, the nanoparticle growth contains six mechanisms, including LaMer-like growth, coalescence, Ostwald ripening, particle (oriented) attachment, adsorbate-induced growth and reaction-induced growth. For each microscopic growth mechanism, the vivid growth scenes of some representative nanomaterials recorded by TEM and SEM measurements are displayed. Afterwards, the scenes from the macroscopic viewpoint for the large submicro- and micro-scale nanospheres and anisotropic nanostructures formation and evolution from one nanostructure into another one are presented. The panorama of how diverse nanomaterials grow during and after laser ablation in liquids shown in this review is intended to offer a overview for researchers to search for the possible mechanisms correlated to their synthesized nanomaterials, and more expectation is desired to better design and tailor the morphology of the nanocrystals synthesized by LAL technique.

laser ablation in liquids, nanoparticle growth mechanism, coalescence, particle attachment, Ostwald ripening, adsorbate-induced growth, reaction-induced growth, self-assembly, self-splitting

PACS number(s): 47.55.nb, 47.20.Ky, 47.11.Fg

Citation: D. S. Zhang, J. Liu, and C. H. Liang, Perspective on how laser-ablated particles grow in liquids, Sci. China-Phys. Mech. Astron. **60**, 074201 (2017), doi: 10.1007/s11433-017-9035-8

1 Introduction

Nanoscience and nanotechnology have entered an era with new findings coming out day by day, mainly driven by their widespread applications in diverse fields, such as biomedicine [1], construction industry [2], flat-panel display and solid state lighting [3], renewable/sustainable energies and sensors [4,5]. To keep pace with the rapid advance in nanoscience and nanotechnology, an increasing number of scientists are now stepping into the nano-world. However, the limited background knowledge of chemistry and materials for non-chemical and non-material scientists hinders their exploration through chemical bottom-up synthesis approaches. Hence, many physical top-bottom techniques are adopted and their prosperity for nanomaterial synthesis is being witnessed.

After more than two decades of development, a newly emerging convenient technique—laser ablation in liquid

*Corresponding authors (DongShi Zhang, email: dongshi17@126.com; ChangHao Liang, email: chliang@issp.ac.cn)

(LAL) has appeared above the horizon with many surprises [6-13]. It is an interdisciplinary technique that integrates optics, chemistry, and physics together. The primary advantage of LAL is its simple setups (a certain volume of liquid, a bulk target and a laser system) which are often easy to be operated allowing nanomaterial synthesis in only one step. Moreover, the LAL-synthesized nanoparticles (NPs) are also advantageous over the chemically-synthesized counterparts from both fundamental and application viewpoints recently reviewed by Zhang et al. [14]. Within, ligand-free feature is the most appealing property, which makes the LAL-synthesized nanomaterials very attractive for catalysis (more active sites) [15], analytic chemistry (featureless spectral background) [16,17], barrierless electrophoresis deposition [18]. All these advantages endowed by LAL are the driving force for its rapid spread all over the globe. Nevertheless, there are still some challenges to be conquered. The dominant one for the fundamental researches is how the nanomaterials nucleate and grow in liquids during and after LAL. Currently, the nucleation process is still shadowed by the black box of the very fast plasma phase. Critical insights can only be gained from the traces of the metastable or growing structures recorded by transmission electron microscopy (TEM) characterization with the aid of other measurements, such as X-ray diffraction (XRD), X-ray photoelectron spectroscopy (XPS) and so on. In this review, we briefly review the progress in this field on the basis of our own perspective and understanding, mainly focusing on the introduction and discussion of the feasible particle growth mechanisms that are responsible for particle growth into various nanostructures.

2 Nanomaterial growth mechanism

Since our perspective on the growth of the LAL-synthesized particles is on the basis of the well-established theories of the wet-chemical synthesis method, here, the particle nucleation-growth routes for the wet-chemical synthesis methods are first introduced in brief. The formation of nanomaterials generally undergoes three stages: (1) nucleation, (2) evolution of nuclei into seeds, and (3) seeds' growth into nanocrystals [19]. Studying particle nucleation (the minuscule clusters consisting of a few atoms and/or ions) is still challenging unless researchers resort to the help of highly advanced microscopies, such as *in situ* TEM. As compared to nucleation studies, the growth mechanisms of nanocrystals under different conditions have been widely investigated and many theories have been proposed, including LaMer growth mechanism, Ostward ripening and digestive ripening, Finke-Watzky two-step mechanism, coalescence, oriented attachment and intraparticle growth [20].

Through correlating the well-known liquid-phase particle growth mechanisms [20] with various LAL-synthesized NPs (NPs) and nanostructures (NSs) [14], we propose that the following mechanisms should explain how NPs and NSs form in liquids during and after LAL, as shown in Figure 1. It also serves as the table of contents for sect. 2, containing the subsections of LaMer-like mechanism (sect. 2.1), coalescence (sect. 2.2), Ostwald ripening (sect. 2.3), particle (oriented) attachment (sect. 2.4), adsorbant-induced growth (sect. 2.5) and reaction-induced growth (sect. 2.6).

2.1 LaMer-like mechanism

LaMer mechanism (Figure 2) is the most frequently adopted concept to explain how particles nucleate and grow in solution, as defined by LaMer's studies on sulfur sols from the decomposition of sodium thiosulfate [21,22]. LaMer mechanism is divided into three stages, as shown in Figure 2,

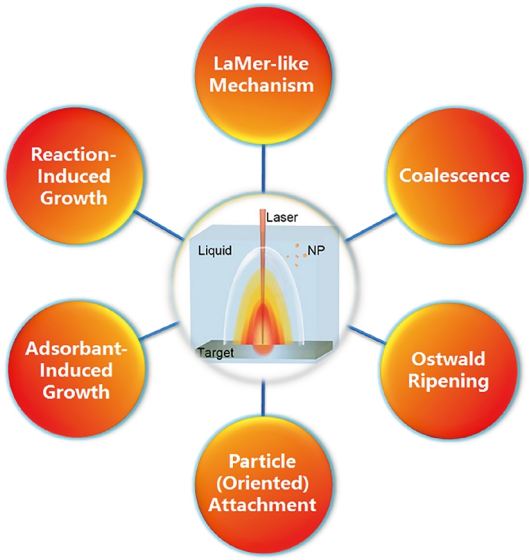

Figure 1 (Color online) Six types of growth mechanisms for the LAL-synthesized NPs.

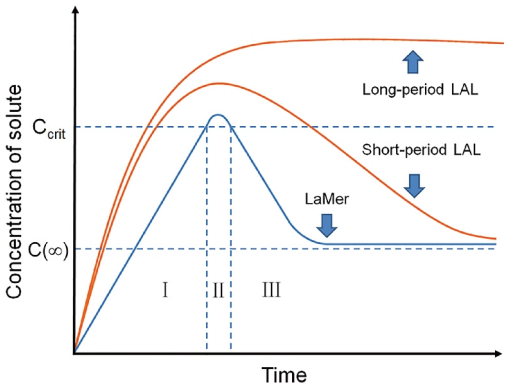

Figure 2 (Color online) LaMer mechanism (blue color) vs. LaMer-like nucleation-growth mechanism (orange color) for the LAL-generated particle. (I) Generation of atoms; (II) self-nucleation; (III) growth.

marked by the blue line: (I) the concentration of free monomers dramatically increases in solution. When the concentration of monomers is well above the critical centration (C_{crit}); (II) the "burst-nucleation" takes place, followed by the subsequent growth process, leading to a significant reduction of the monomers' concentration and (III) finally the seed's concentration stays at a value (C_∞) far below C_{crit}. Note that when the concentration drops below C_{crit}, there will be almost no occurrence of nucleation due to the low concentration of monomers far below the one required for nucleation. In big difference as compared to LaMer mechanism, there are two routes for particle growth while implementing LAL, including long-period laser ablation and short-period laser ablation in terms of different particle-supply period (Figure 2). The outlines of the LaMer-like curves for the long-period LAL-synthesized particles are deduced from the LAL productivity over a long period. Schwenke's group [23] and Sarraf's group [24] investigated the long-period LAL productivity and characterized the ablated mass and the peak intensity of the colloids in UV-vis spectra, respectively. They both found that the colloids' concentration gradually became saturated when the LAL lasted for more than 30 minutes in batch chambers (Figure 3). This is because of the fact that when the particles' concentration increases, the consumption of laser energy by the colloids' absorption and refraction is enhanced [25], thus leading to a decrease in the laser energy arrival at the target, this phenomenon has been discussed in detail in ref. [14]. Differentiation between "short-period" and "long-period" is difficult because of the synergistic effect of each factor in the liquid-laser-process-target system. For high-power and high-repetition-rate lasers, the time for colloids to become saturated will be dramatically reduced. In our opinion, in tens of milliliter liquid, LAL which lasts for more than half an hour can be classified as long-period LAL, while no more than several minutes LAL can be defined as short-period LAL. Note that while taking use of flowing liquid [26], the concentration of colloids is almost constant and particle growth will follow the short-period LAL curve.

To better understand the short-period LAL curve shown in Figure 2, the LAL panaroma (Figure 4) [27] for particle nucleation and growth is introduced first. When a laser pulse with sufficient energy (above the ablation threshold of the

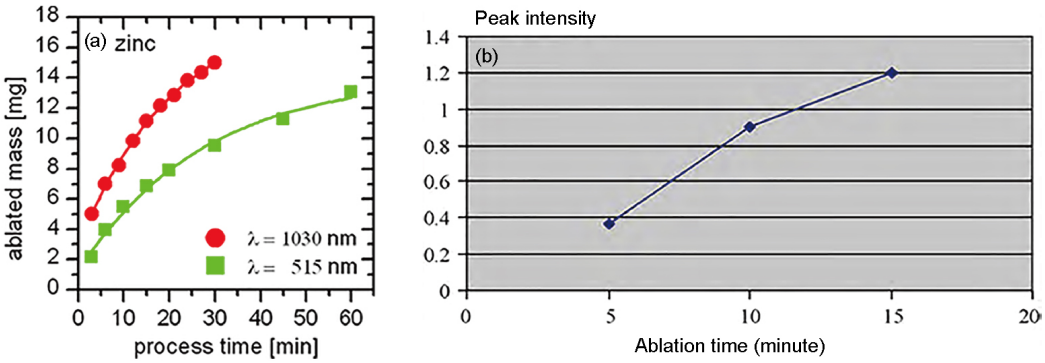

Figure 3 (Color online) LAL productivity as a function of process (ablation) time. (a) Cumulative ablated mass over processing time of zinc for ablation in tetrahydrofuran (THF) using fundamental (1030 nm;250 μJ) and second harmonic (515 nm;125 μJ) laser wavelengths. Reprinted with permission from ref. [23]. Copyright 2011 Springer; (b) UV-visible absorption peak intensity versus ablation time for colloidal solutions synthesized by LAL of Al in ethanol (λ=1064 nm,E=280 mJ/pulse). Reprinted with permission from ref. [24]. Copyright 2010 Elsevier.

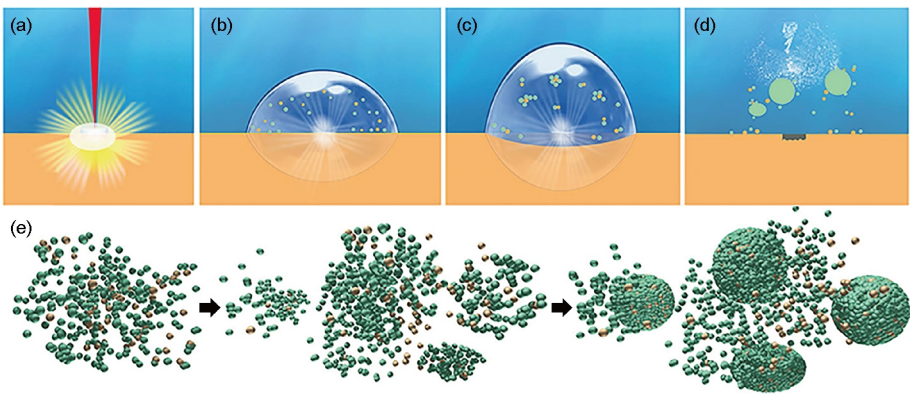

Figure 4 (Color online) LAL processes as illustrated by one pulse ablation. (a) Plasma generation; (b) bubble generation during plasma quenching; (c) bubble oscillation; (d) bubble collapse releasing active tiny particle in the liquid; (e) atoms' nucleation into nuclei during the plasma-bubble phases. Reprinted with permission from ref. [27]. Copyright 2015 Nature Publishing Group.

target material) interacts with the target material, a high-temperature (up to 7000 K [28]) and high-pressure plasma (up to 15 GPa) is generated (Figure 4(a)), which will cause the atomization and ionization of the target materials as well as the decomposition of liquid molecules [8]. Then plasma undergoes rapid quenching, during which time its energy is transferred to the surrounding liquid and leads to the formation of a cavitation bubble (Figure 4(b)). Note that chemical reactions may take place between the target-ejected materials and the decomposed liquid molecules or between the reactive species originating from the targets during plasma generation-quenching processes [29], mostly probable at plasma-liquid interfacial region, which is the reason why oxide [30], carbide [31,32], sulfide [33], nitride [34] and hydroxide [35] nanomaterials are achievable by LAL. Rapid nucleation of the atoms and ions into nucleus [36] may occur at the end of plasma phase and initial stage of bubble phase. Considering the very high collision rate of the nuclei due to the high amount of the generated species (10^{20} cm^{-3} [37]), the nuclei will rapidly transform into particles (Figure 4(e)). So tiny particles in majority and big particles in minority [38,39] can be detected in the cavitation bubble by scanning small-angle X-ray scattering (SAXS). The cavitation bubble will experience a series of expansion-shrink fluctuation (Figure 4(b) and (c)) [14] and when the bubble collapses these particles are released in the liquids (Figure 4(d)) [38-40]. Since these ligand-free particles are very active they will act as the building blocks to form a large variety of spherical and unspherical nanomaterials [14].

As seen, each pulse's interaction with the material target will trigger a nucleation-growth process of the ejected materials. Hence, the time required for LAL to reach C_{cri} is shorter than that of the wet-chemical synthesis method, as shown in Figure 2, no matter it is long-period LAL or short-period LAL. Meanwhile, on the basis of the literature which shows the possibility of particle-ripening behavior for several weeks [41] and considering the slow motility of the active particles in the aging static liquid, the time required for termination of the particle growth should be longer than that of the conventional LaMer mechanism. The time scale for short-period LAL is roughly defined from several seconds to several minutes as most groups adopted for particle characterization and analysis [42-44]. Hence, tailoring the ablation period for the settled liquid-target-process-laser system allows one to tailor the active-particle concentration and control the particles' growth.

Why is it necessary to differentiate short-period and long-period LAL to manipulate the particle concentration? It lies in concentration-dependent nanomaterial evolution. Taking the LAL-obtained Mn_3O_4 products for example, long-period picosecond laser (40 min) ablation of a pure Mn target in 30 mL water can trigger a second-stage growth of 90-170 nm hollow particles (Figure 5(c), (d)) consisting of

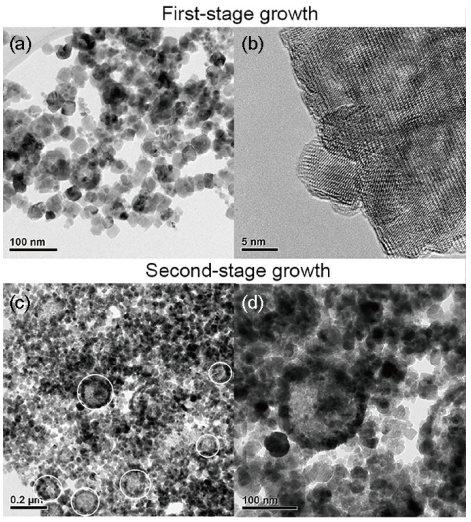

Figure 5 Two stage growth after long-period LAL. (a) and (b) first-stage grown Mn_3O_4 nanocubes; (c) and (d) second-stage growth of the nanocube-assembled larger hollow particles. Adapted with permission from ref. [30]. Copyright 2017 Wiley-VCH.

the first-stage grown 20-30 nm nanocubes (Figure 5(a) and (b)) [30]. The hollow spheres are appealing for catalytic applications, but are difficult to be obtained by conventional wet-chemical synthesis method. The assembly of cubic Mn_3O_4 particles into large hollow particles may be because of high concentration of cubic Mn_3O_4 particles well above the C_{crit} in which case a second stage growth is "switched on" with the cubic Mn_3O_4 particles as building blocks. Other supports of the benefit of long-period LAL for unique nanostructures (nanoflower and nanoleaf) can be found in sect. 3.3. Hence, adjusting the time-period of LAL enables one to control the particle "seed" concentration in liquids and meanwhile offers new opportunities to switch on multiple growth stages of seeds growth for novel structure synthesis.

For short-period LAL, the melting/fragmentation (LML/LFL) processes in the beam path (Figure 6) accompanied by LAL may not dominate the products even though they are an underlying reason for the bimodal size distribution of the LAL-synthesized particles [14]. But when implementing long-period LAL, LML and LFL side processes cannot be neglected. Yan et al. [45] showed that 20-min LAL of $Ni_{81}Fe_{19}$ in sodium dodecyl sulfate (SDS) aqueous solution only gave birth to tiny particles, while 4-h LAL caused the assembly and sintering of particles into sub-micro- to micro-scale hollow spheres. Further extending the LAL period to 9 h induced the fragmentation of the big particles into tiny particles with the size less than 100 nm [45]. Note that long-period LAL even allows downsize of the LAL-synthesized particles to quantum dots (QDs), which is the reason why Xin et al. [46] extended LAL for 8 h to obtain sufficient amount of Si QDs for constructing hybrid inorganic/organic light-emitting diode (LED).

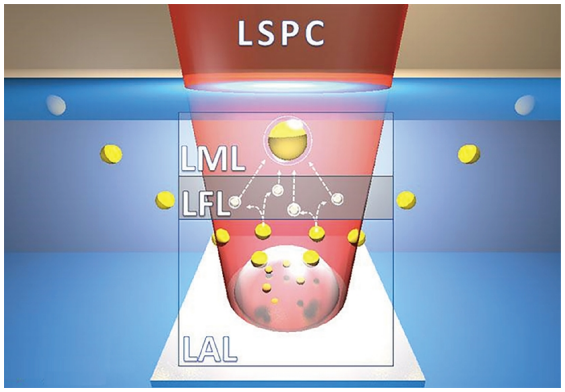

Figure 6 (Color online) LML and LFL side processes accompanied by LAL because of the variation in laser fluence along the beam path in liquid. Reprinted with permission from ref. [14]. Copyright 2017 American Chemical Society.

2.2 Coalescence

Coalescence of small unites into bigger ones is a natural phenomenon triggered by either Brownian or gravitational or thermocapillary motion [47]. In nanoscience, it is often the Brownian motion [48] that leads to the coalescence of randomly attached (aggregated) seeds or particles. As for LAL, at the initial stage of bubble phase, high Brownian collision rates resulting from the plasma-induced large amounts of atoms facilitate the coalescence of atoms into nuclei. For the particle growth in the liquid phase, coalescence occurs because of the laser-driven melting (coalescence) behavior when the colloids appear in the laser path [49,50]. Figure 7 depicts the LAL-involving coalescence process while treating the CuN or Cu_3N micropowder suspensions [49]. As seen, at the beginning, LAL generates small particles with primary size less than 5 nm. Then, these small particles aggregate/agglomerate. The NP aggregation/agglomeration may either be triggered by the instability of the NPs [51] or being pushed together by the bubble collapse-induced shockwave [52]. When the aggregated/agglomerated NPs appear in the beam path, they absorb laser energy and change into large particles by the coalescence process [49]. This scenario is similar to LML, which excels at fusing small particles together to enlarge the particles [52,53]. When diffusion coalescence happens, the particles may become monocrystalline, but in most cases, the synthesized particles are polycrystalline [54,55] with obvious grain boundaries, which can be clarified by analysis of crystal planes based on high-resolution transmission electron microscopy (HRTEM) and selected area electron diffraction (SAED) characterization. Shen's group [56,57] has done a series of works in this field and confirmed the coalescence behaviors of the LAL-synthesized TiO_2, Ni-doped γ-Al_2O_3 [58] and Mg-doped $Co_{3-\delta}O_4$ spinel NPs [59].

Coalescence process plays the dominant role in the formation of alloy particles during LAL and the nanoalloys always turn out to be segregated, biphase and core-shell morphologies (Figure 8(a)-(c)) [60]. Malviya et al. [60,61] reported that the LAL-obtained $Ag_{40}Cu_{60}$ alloy particles are composed of many nanosized grains with sizes of ~3±0.5 nm (Figure 8(b)) due to the large size differences (Ag:Cu=144:128; pm) in the silver and copper atoms. These segregated alloy particles with enormous grains are unstable and will recrystallize upon *in-situ* TEM heating [61]. During their recrystallization, concurrent diffusion-induced Ag-Cu phase separation and growth give rise to the formation of Janus-like biphase particles. Interestingly, the large segregated alloy particles (~40 nm) experience a metastable state of Cu@Ag core-shell morphology during their evolution into the biphase particles. This finding indicates the possible phase transformation of alloy NPs from segregated to core-shell and core-shell to biphase upon laser irradiation because laser irradiation can behave like *in situ* TEM heating to heat the NPs up to hundreds of °C and even higher, as confirmed by NP reshaping and melting behaviors [52,62]. The formation of core-shell nanoalloy is triggered by the lower surface energy of Ag (1.25 J/m^2) as compared to Cu (1.85 J/m^2) [63], which makes Ag grains of large particles preferentially grow along the particle's surface to form Cu@Ag core-shell structures rather than Ag@Cu structures.

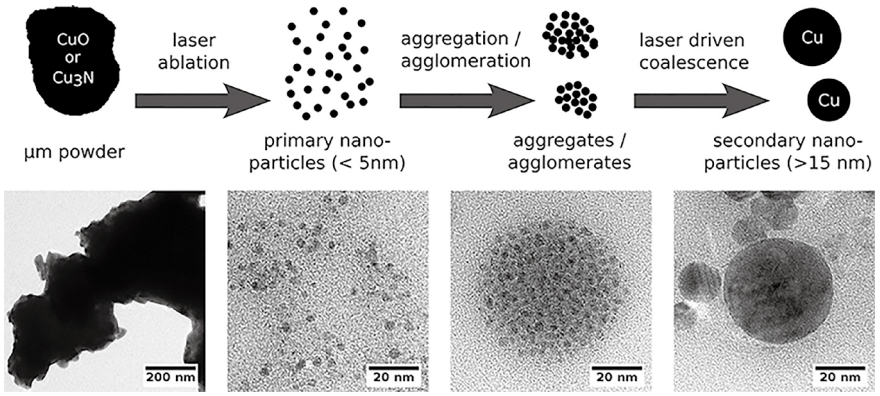

Figure 7 Laser driven coalescence of particle aggregates/agglomerates into bigger particles. Reprinted with permission from ref. [49]. Copyright 2014 American Chemical Society.

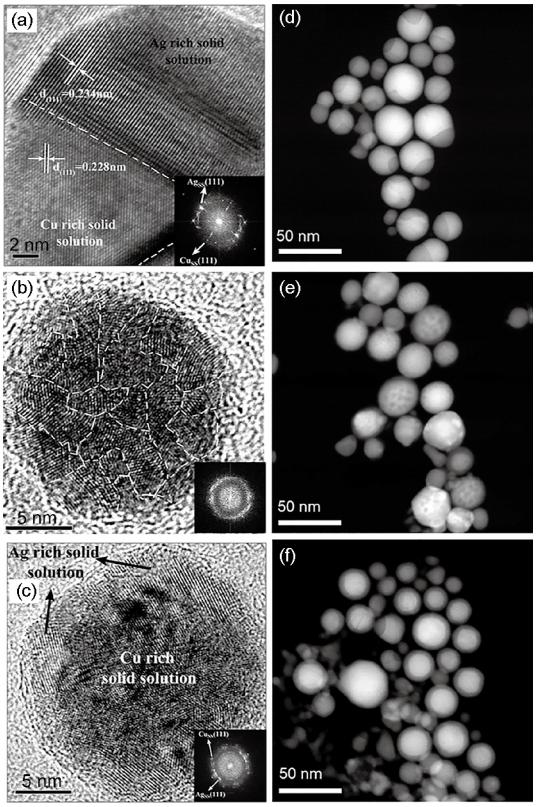

Figure 8 LAL-induced coalescence of metal materials into nanoalloy. (a)-(c) Representative HRTEM micrograph of the synthesized alloy NPs from four different target compositions, namely, Ag-X atom % Cu (X=40, 60, 80). Inset shows the fast Fourier transform (FFT) of the particle and corresponding (d)-(f) high angle angular dark field (HAADF) images of the LAL-synthesized nanoalloys. Reprinted with permission from ref. [60]. Copyright 2014 American Chemical Society.

The formation of Cu@Ag core-shell is particularly obvious for Ag-rich AgCu alloy particles (Figure 8(f)) [60]. Similarly, lower surface energy of Au (1.50 J/m^2) as compared to Fe (2.42-2.48 J/m^2) leads to the formation of the LAL-synthesized Fe@Au alloy particles [64]. Since the surface energy varies with the particle size and composition and considering the different heating degrees of laser irradiation for each coalesced alloy NP, the LAL-synthesized alloys NPs are normally the mixtures of the segregated and biphase NPs (Figure 8(d)) or the mixtures of the segregated and core-shell NPs (Figure 8(e)) or the mixtures of the core-shell and biphase NPs (Figure 8(f)) [60].

Liu et al. [65] reported the spontaneous growth of the LAL-synthesized Ge nanoparticles and during this process the particles' phase also changed, as shown in Figure 9. Specifically, at the beginning, the LAL-synthesized small Ge NPs of 7-8 nm were in a metastable state with an amorphous phase. Aging the colloids in water at the ambient temperature resulted in the aggregation of the Ge NPs with size approximate to 100 nm at 3 h (Figure 9(d)). These Ge aggregates further evolved into submicrospheres with average size of 350 nm after 24 h aging. Interestingly, both XRD and SAED diffraction rings (Figure 9(e)) and HRTEM plane analysis reveal that the Ge aggregates obtained after 3 h aging are in a high-pressure tetragonal and/or cubic phase (Figure 9(j)). This finding indicates that for Ge NPs, the amorphous phase is an intermediate precursor of the high-pressure phase, in accordance with previous reports [66], thus shedding light on the ubiquitous amorphization phenomenon during LAL [67-69]. Hence, besides giving a hint on the coalescence process for particle growth, this work is of great importance for demonstrating the possibility of phase variation during particle growth, which should deserve the researchers' attention while preserving the colloids in liquid for a long period (>3 h).

2.3 Ostwald ripening

Ostwald ripening (also termed as coarsening) is a process that describes the big particle growth at the expense of smaller particles' dissolution at the big ones' surfaces [70]. The mathematical theory for Ostwald ripening has been proposed by Lifshitz and Slyozov [71] and independently by Wagner [72]. Hence, the combined models are termed as LSW theory and have been extensively adopted for understanding how particles grow [70,73]. According to the LSW theory, the particle radius increases with the elapsed time, following eq. (1).

$$r = r_0 + ct^{1/3}, \tag{1}$$

where r is the mean particle radius, r_0 is the initial particle radius, c is the material constant, t is the elapsed time. Since the normally characterized LAL-synthesized NPs are the ones after growth, limited hints can be gained to verify whether the time-dependent growth of the LAL-synthesized particles fits the trend of Ostwald ripening. To solve this problem, Jendrzej et al. [74] fragmented the LAL-synthesized Pt NPs into naked atom clusters to mimic the initial stage of LAL and characterized their growth kinetic. The results show that both the coalescence and Ostwald ripening are responsible for the particle growth of Pt NPs, based on which they proposed two growth routes for the naked clusters (Figure 10). One is ripening of tiny particles into bigger ones, the other is a successive coagulation-coalseconce-agglomeration growth process chain. The time-dependent barrierless coalescence model of eq. (2) used for their theoretical fitting is proposed by Riberio et al. [75] on the basis of the Smoluchowsky coagulation:

$$r = r_0\left(\frac{2k_0t+1}{kc_0t+1}\right)^{1/3}, \tag{2}$$

where r is the mean particle radius, r_0 is the initial particle radius, t is the elapsed time, c_0 is the initial particle concentration and k is the rate constant. It is clear that an initial rapid growth followed by a slow growth in the liquid phase should dominate the particle growth of metallic particles after LAL. The particle coalescence and Ostwald ripening are able to

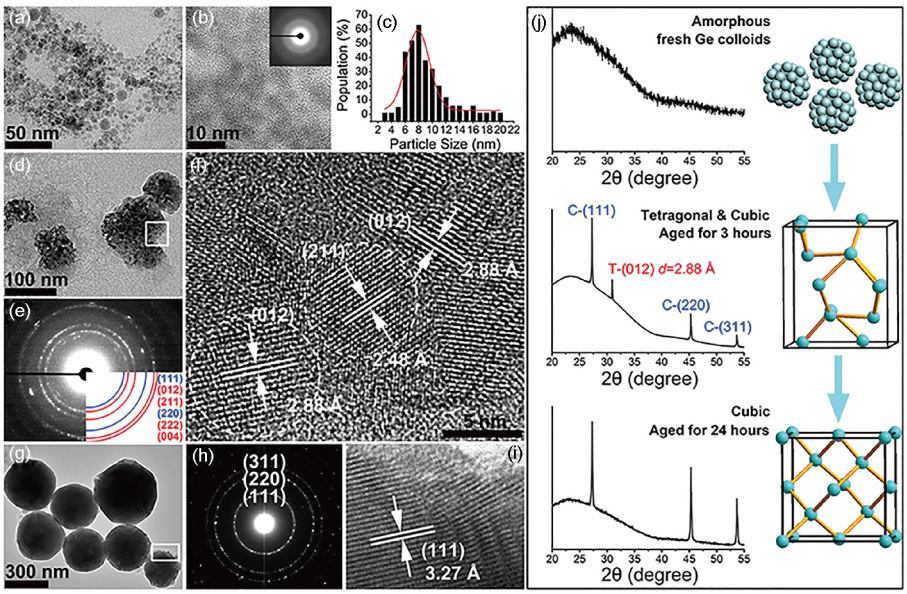

Figure 9 (Color online) Aging induced self-coalescence of small particles into submicrospheres. (a) TEM images of fresh Ge NPs, with inset in (b) the corresponding SAED pattern; (c) size histogram of fresh Ge NPs; (d)-(f) low-magnification TEM image, selected-area electron diffraction (SAED) pattern, and HRTEM image of the selected area in (d) for Ge NPs with aging time of 3 h; (g)-(i) low-magnification TEM image, SAED pattern, and HRTEM image of the selected area in (g) for Ge NPs with aging time of 24 h; (j) XRD patterns of Ge NPs with different aging time. Adapted with permission from ref. [65]. Copyright 2013 Nature Publishing Group.

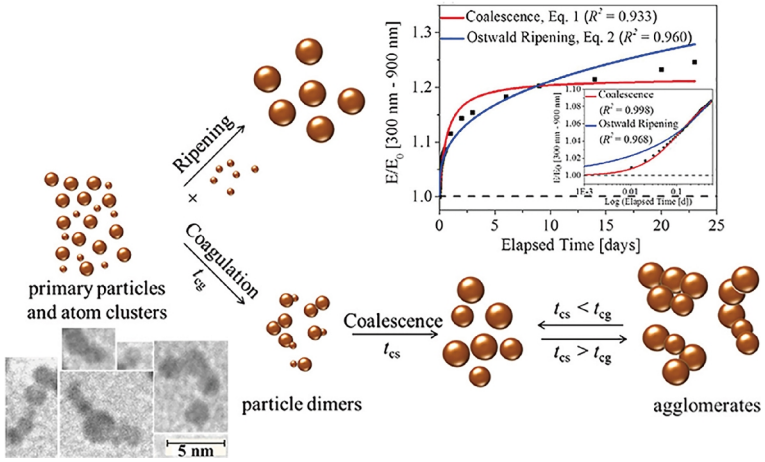

Figure 10 (Color online) Schematic figure of growth kinetics by combined Ostwald ripening and coalescence of tiny Pt colloids in water and exemplarily shown TEM image of Pt atom clusters together with the confirmation of concurrence of coalescence. Inset figure: Ostwald ripening by fitting the experimental data to eqs. (1) and (2) for a short time range from 0 to 13 h. Adapted with permission from ref. [74]. Copyright 2016 Elsevier.

last for almost one month or even longer. Interestingly, through the coalescence route, the tiny clusters can spontaneously grow into nanochains [74,76], while through Ostwald ripening, large particles are the final products. That is why sometimes particles together with nanochains are both observed after LAL [77].

2.4 Particle (oriented) attachment

Crystallization by particle attachment is a common phenomenon in synthetic, biogenic, and geologic environments for ions, atoms, and molecules to evolve into crystal nanomaterials [78]. Oriented attachment (OA) refers to the alignment of different crystal particles along their crystallographic planes. It is considered that van der Waals interactions, Coulombic interactions, and dipolar interactions facilitate crystallographic oriented attachment of inorganic particles in proximity [79]. Besides the oriented attachment route, there are many other particle-attachment routes to explain why poorly crystalline NPs and amorphous NPs can evolve into bulk crystal on the basis of both the free-energy landscapes and the reaction dynamics that govern particle formation and interaction [78]. Note that the occurrence of particle attachment process cannot rule out the possibility of other growth mechanisms, such as Ostwald ripening, because particle solubility is high for small particles according to the

Gibbs-Thomson relation [70] which may cause the dissolution of tiny particles by the larger ones.

It is because of the lack of HRTEM characterization of the crystal planes that make the applicability of particle attachment mechanism to the LAL-synthesized nanomaterials unveil two decades after the first reports of LAL in 1993 [80,81]. For instance, Wu et al. [82] reported the special grain boundaries of anatase nanocondensates stemming from the oriented attachment by LAL of Ti in tetraethyl orthosilicate (TEOS), including the symmetrical [100] tilt boundaries with (001) or $(01\bar{1})$ interfaces and an asymmetrical $[1\bar{1}0]$ tilt boundary with a (001)/$(11\bar{2})$ heterointerface. Liu et al. [41] reported that the uncapped Te NPs synthesized in five solutions (water, methanol, ethanol, acetone and dichloromethane) attached with each other along their crystallographic planes, which is also in accordance with the oriented attachment mechanism [79]. In water, the particles attach along the (101) plane with a lattice spacing of 0.323 nm (Figure 11(a)) and the crystal boundary is clear to be differentiated [41]. Hsu et al. [83] observed a slight diffraction splitting of the upper left and lower right parts of one LAL-synthesized C–Si–H-doped $Co_{1-x}O$ particle and attributed deviation to a minor misorientation of the two attached particles during their oriented attachment over their (100) surfaces. Wang et al. and Lin et al. proposed that the oriented attachment mechanism facilitates the formation of the LAL-obtained YVO_4:Eu^{3+} ovoid-like nanostructures [84] and CuO nanospindles [85], respectively.

From the above-mentioned examples, it seems that LAL particles should most properly follow the oriented attachment or nearly oriented particle attachment route. But in reality, it is not the case. Zhang et al. [30] observed that the building particle units (~5 nm) shown in Figure 11(b) and (c) for Mn_3O_4 nanosheets and Mn_3O_4 nanofibers are not crystallized, which does not obey the oriented attachment. Nevertheless, the traces of tiny particles on the highly crystalline nanosheets (Figure 11(c)) which are the simultaneous LAL products of nanofibers, give strong evidence of the crystallization by particle attachment. Particle growth on different layers of the nanostructure will leads to the increase in the thickness of nanosheets and nanofibers [30]. These findings well explain why the partially crystalline or amorphous particles can evolve into the crystalline particles. Therefore, the particle attachment rather than oriented attachment should be a ubiquitous phenomenon for the evolution of the LAL-synthesized particles into nonspherical nanostructures.

It has been well-recognized that highly charged small NPs endowed by surfactants have strong columbic interactions which will strongly affect the kinetics of the OA process and even inhibit the growth of long nanostructures [79]. However, this adverse effect is not so apparent for the LAL-synthesized NPs because Mn_3O_4 nanosheets and nanofibers [30] with length of several micrometers have been synthesized by LAL following the particle attachment mechanism. The following factors should be the reasons to explain such phenomenon. (1) In most cases, the surface charge of LAL-synthesized particles is often measured after their growth, which cannot rule out the possibility that the small particles are not charged enough after LAL, making them easily get close to each other to get attached. (2) Generally, the LAL-synthesized NPs are rich with uncoordinated sites which can easily absorb or bond with the surrounding species. These species may be either solvent molecules themselves or the decomposed species, such as enolate [86] and polyyne [87], or ions (see sect. 2.5) because adsorbate the nucleation of clusters to enable them to grow sufficiently fast rather than coagulate together [88]. (3) Reports have shown that high-temperature colloidal solution is more thermodynamically favorable to the occurrence of particles' attachment to form long nanostructures [89,90]. Since every laser pulse's interaction with the target generates plasma whose rapid quenching transmits heat to the surrounding liquid and heat transfer can take place to the laser irradiated particles in the beam path, the colloidal temperature increases [91]. Hence, long-period LAL often gives rise to an increase of the liquid's temperature and leads to the acceleration of the particle attachment even though the particles are highly charged.

2.5 Adsorbate-induced growth

Nowadays, growth-directing adsorbates (surfactants or ions) are popular to be used to synthesize different shapes of nanomaterials by influencing the growth kinetics of nanocrystals [92] because in presence of strongly-charged surface adsorbates, Ostwald ripening growth is inhibited. When it comes to LAL, their roles are compromised because in most applications, the naked surface of the nanoproducts is favored without addition of the surfactants [93], that is why LAL is often recommended for its surfactant-free [94,95] or ligand-free [16,96-99] feature. This does not mean that surfactants are not welcome for LAL. In reality, surfactants are often used to enhance the stability [100] or control size distribution [101] or tune the phase [102,103] and surface state [104,105] of the obtained particles. Although selective adsorption of the surfactants on the LAL-generated seeds is very difficult due to the extreme condition (high-temperature and high-pressure) induced during plasma generation and rapid plasma quenching, they can induce self-assembly of the LAL-obtained particles into anisotropic nanostructures while aging the surfactant-containing colloidal solutions. For example, aging the ZnO colloids which were synthesized by LAL of Zn in cetyl trimethylammonium bromide (CTAB) aqueous solution (1.0×10^{-3} M) for 7 days allows the formation of spindle-like structure [106]. Huang et al. [107] showed that the LAL-obtained amorphous structures gradually evolved into spindle-like GaOOH in CTAB aqueous solution (Figure 12).

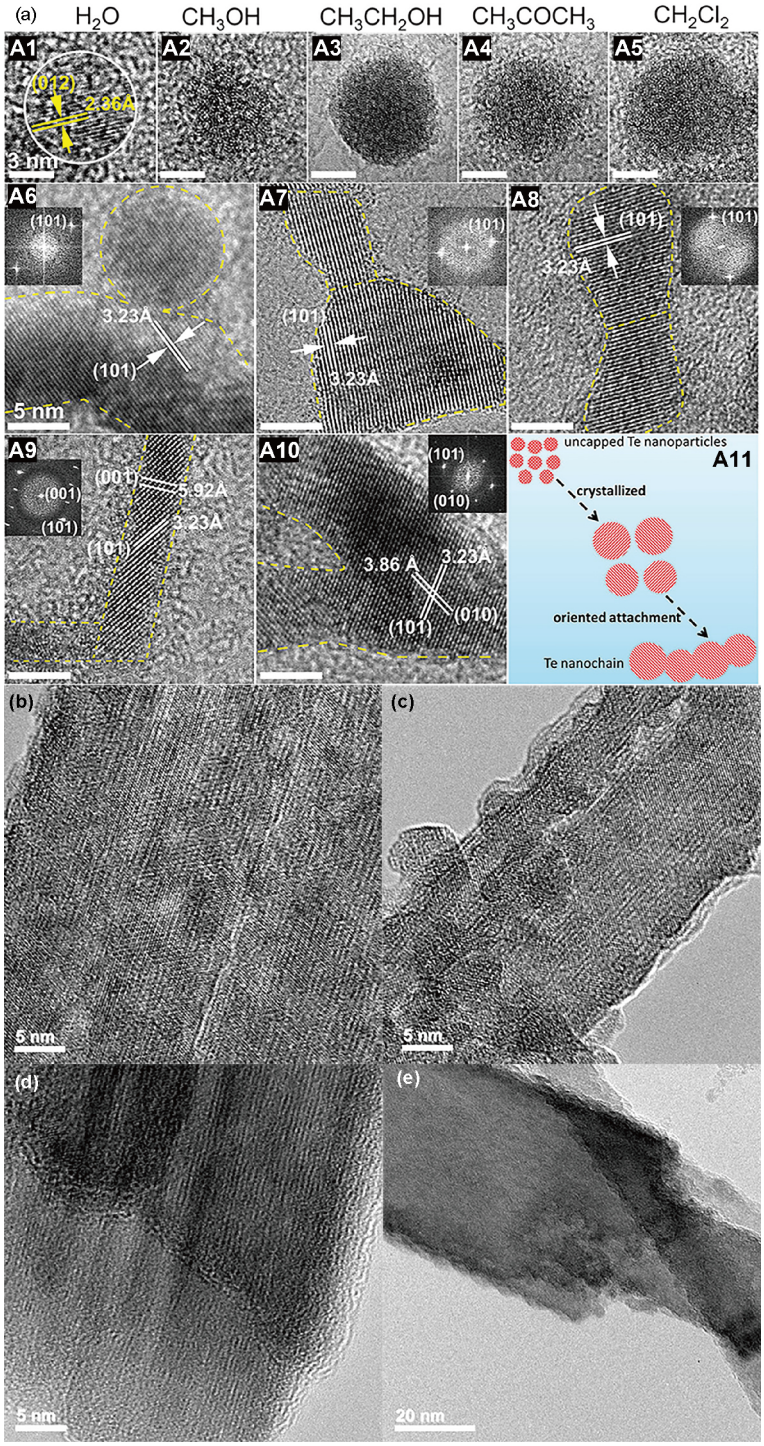

Figure 11 (Color online) (a) HRTEM images of an individual uncapped Te NP (A1-A5) and sectional Te nanochain (A6-A10) in H_2O, CH_3OH, CH_3CH_2OH, CH_3COCH_3, and CH_2Cl_2. Scale bar: 3 nm for A1-A5; 5 nm for A6-A10. (A11) Formation of Te nanochains dominated by the typical oriented attachment (OA) growth mechanism. Adapted from permission from ref. [41]. Copyright 2016 Nature Publishing Group. (b), (c) HRTEM images of a Mn_3O_4 nanosheet and a Mn_3O_4 nanofiber synthesized by LAL of Mn in water-ethanol mixture with volume ratio of 1:2; (d), (e) layered growth of nanosheets and nanofibers for thickness increase. Reprinted from permission from ref. [30]. Copyright 2017 Wiley-VCH.

Liang et al. [35] collected $Mg(OH)_2$ nanostructures with tube-, rod- or platelet-like morphologies 6 h aging after LAL of Mg in SDS aqueous solution. Note that sometimes, the surfactants are capable of reacting with the LAL-generated species, resulting in the formation of novel nanostructures. For instance, while implementing LAL of Zn in SDS solution, the charged DS ions directly bond with the zinc-coordinated sites of Zn hydroxides to prevent their dehydration into ZnO and as a result, ZnDS platelets are generated [108,109].

Besides surfactants, ions which have affinity to certain

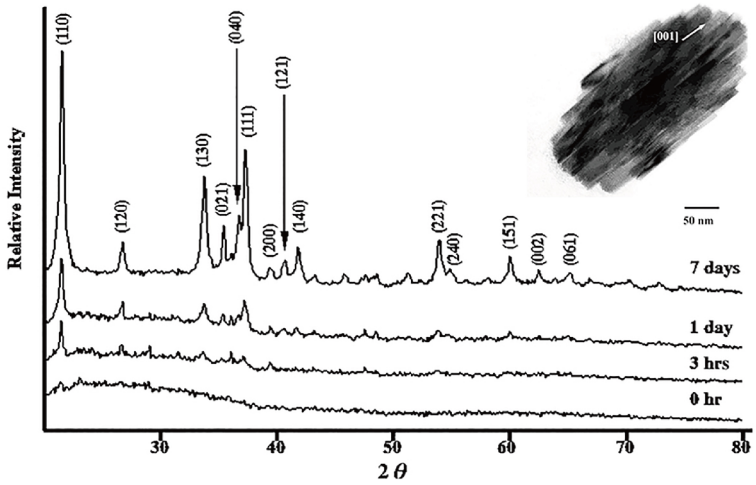

Figure 12 Adsorbates of surfactants and ions induced particle growth during aging. Aging induced colloidal phase transition into spindle-like GaOOH from amorphous structures, which are synthesized by LAL of Ga in an aqueous solution of 2.2×10^{-3} M CTAB for 20 min exposure time. Reprinted from permission of ref. [107]. Copyright 2004 American Chemical Society.

facets of the particles are also extensively used to manipulate the particle shape. Although various salts are employed as the additive for LAL, in most cases, they act as the size quenching agents to inhibit NP growth by enhancing the NP surface charge [94,110,111]. Zhang et al. [30] verified that the adsorption of Fe^{3+} ions on manganese oxides benefits the formation of nanosheets and nanofibers, which will be introduced in sect. 3.2. Park's group [112] has also proven the possibility of controlling the particle shape by ion adsorbates. Triangular nanoplates appear after 24 h aging the Au colloids which were obtained by LAL of Au in NaI solution [112]. The formation of Au nanoplates is due to the higher affinity of iodide ions to the Au (111) than other facets such as (110) and (100) [113]. But the nanoplates are not uniform and the size is in a wide range from tens of nanometers to several hundreds of nanometers, similar to the state of the cubic NiO [114] and conical $Al(OH)_3$ [103] particles generated by SDS-aided and CTAB-aided growth, respectively. Hence, it can be concluded that the ion-adsorbate directed growth proceeds at a nonuniform pace for different particles due to different local concentrations aggregation states of the LAL-synthesized particles.

2.6 Reaction-induced growth

The reaction-growth mechanism is proposed since the chemical reaction often contributes to the *in situ* growth of the LAL-synthesized particles. This should thanks to the generation of new species (e.g., atoms, ions and clusters) are generated after each pulse ablation due to the atomization and ionization of the target materials. If these newly formed species are able to interact with each other or afore added ions in liquid or with the already formed nuclei or particle seeds, novel nanomaterials may come out. A representative is the discovery of novel football-like microspheres allowing *in situ* growth up to 2-7 μm (Figure 13(a)-(c)) which are captured by the microstructures induced by laser ablation of Ag-doped germanium wafers in water [27]. Interestingly, the AgGe microspheres are Ag-rich with the Ag up to 80 wt% (Figure 13(d)-(f)), in big difference with its low ratio (0.07 wt%) in the Ge wafer. Therefore, a new particle formation is anticipated. After checking the intermediate structures, the authors get some clues to clarify the key factors to give rise to the formation of such AgGe microspheres. The high pressure and high temperature of the plasma causes the atomization and ionization of both Ag and Ge target materials. Since Ge is a good nucleating agent for Ag [115], AgGe nuclei rapidly form during the plasma quenching. Since there is a galvanic reaction between Ge and Ag^+, those nucleated Ge will be replaced by Ag through the reaction of $4Ag^{+}+Ge\rightarrow4Ag+Ge^{4+}$. Such reaction also takes place after the AgGe nuclei are released into the liquid and hence leads to the formation of Ag-rich particles. Because each pulse ablation supplies a certain amount of Ag^+ ions in liquid, and those Ge atoms or particles newly anchored on the already formed AgGe particles induced by the bubble-collapse induced shockwave facilitate the surface layered growth of the Ag, as shown in Figure 13(g)-(j). These novel football-like microspheres are difficult to be obtained by wet-chemical synthesis method because once the outmost Ge atoms are consumed; it is difficult to introduce new Ge atoms on the Ag surfaces, also confirmed by the authors [27]. Hence, it can be concluded that LAL allows continuous supply of the reactive species for long-period reactions, which may stimulate more novel nanomaterials to be produced.

Active salt additives are also good candidates to induce *in situ* growth of composites and alloy particles. Jiménez et al. [116] successfully synthesized SiO_2-capped noble metal (Ag, Au and Ag-Au mixture) NPs in a single step by LAL of Si in $AgNO_3$, $HAuCl_4$, and $AgNO_3$-$HAuCl_4$ mixtures, where *in*

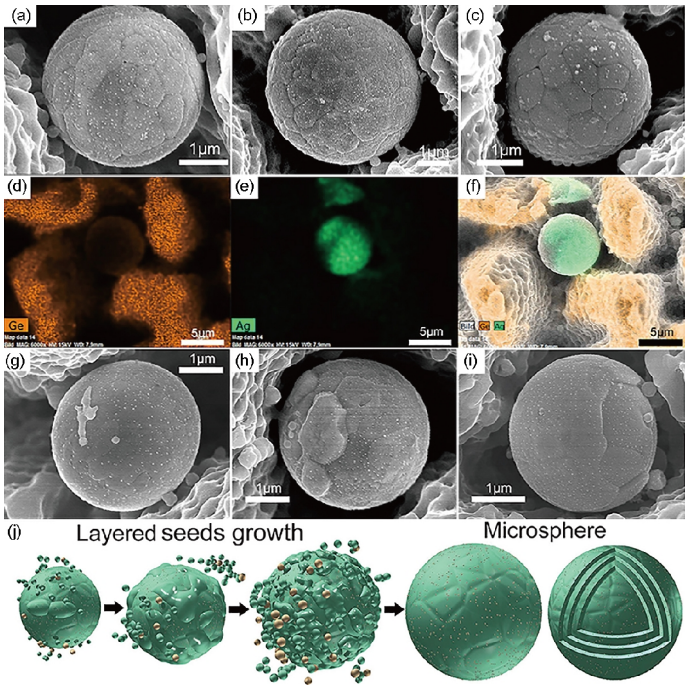

Figure 13 (Color online) Football-like microspheres obtained by laser ablation of Ag-doped Ge wafers in water. (a)-(c) The morphology of the microspheres; (d)-(f) energy dispersive X-ray spectroscopy (EDX) mapping of the microspheres; (g)-(i) the scanning electron microscope (SEM) evidence to support the layered growth mechanism; (j) schematic of layered seeds growth mechanism. Adapted from permission of ref. [27]. Copyright 2015 Nature Publishing Group.

situ reduction of Ag^+ and $AuCl_4^-$ into metal NPs by the LAL-generated Si NPs occurred. Mukherjee group obtained CoPt alloy NPs taking advantage of the galvanic replacement reaction of $Co+Pt^{2+}\rightarrow Co^{2+}+Pt$ by LAL of Co in K_2PtCl_4 solution and subsequent laser irradiation induced particle alloying [117]. Similarly, Park et al. [118] developed PdCu alloy NPs by LAL of Pd in $CuCl_2$ solution on the basis of the galvanic replacement reaction between the ablated Pd NPs and Cu^{2+} ions. As seen, the ion additives offer many opportunities for the occurrence of *in situ* reactions during LAL to induce *in situ* growth of the particles, especially attractive for one-step synthesis of alloy particles.

3 Self-assembly and self-splitting

In the last section, we have introduced six particle formation mechanisms from the microscopic viewpoint, mainly focusing on how tiny particles nucleate and interact with each other. However, these mechanisms cannot explain how submicron particles and anisotropic nanostructures form. Hence, in this section, from the macroscopic viewpoint, the growth processes of submicrospheres, nanosheets and nanofibers and nanospindles are presented.

3.1 Submicrospheres

Submicrospheres are sometimes found after LAL [119], especially those experiments performed using nanosecond lasers. Particle attachment followed by Ostwald ripening should be the main growth route for the formation of submicrospheres, as confirmed by Liu et al. [41] who observed gradual growth of tiny Te particles into larger ones while aging the colloids in different solvents (water, methanol, ethanol, acetone and dichloromethane), as shown in Figure 14. At the beginning (2 s), the particles in the liquids are tiny with the average size of 2 nm. As time passes by, long nanochains consisting of tiny particles are observed and interestingly, these chains have many branches in different directions. These chains form following the particle attachment mechanism. When aging the colloids in liquid for hours or days or a week, these trains transform into nanoparticle aggregation and certain parts of the nanochains become bigger and evolve into larger NPs with the average size of ~20 nm except the case of particles in dichloromethane where the chains transform into large nanocubes with the size of ~200 nm [41]. Further elongating the aging time makes the particles become mature and all of them transform into large submicrospheres (in H_2O) or microspheres (other liquids). It is clearly seen that the growth rates of Te nanochains formation in different solvents are different following the order: $H_2O>CH_3OH>CH_3COCH_3>CH_3CH_2OH>CH_2Cl_2$. Deduced from the experimental trend and Derjaguin-Landau-Verwey-Overbeek (DLVO) theory, the authors concluded that the growth kinetics strongly depend on the polarity and dielectric constant of solvent molecules, but are more associated with the NP surface charge, that is, NP stability. High

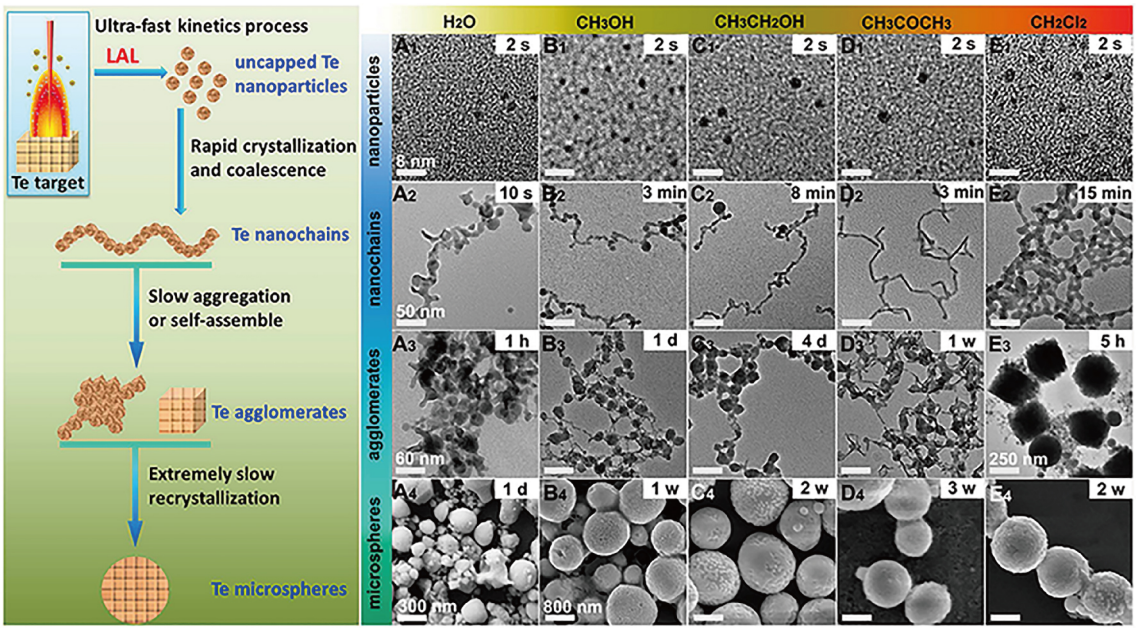

Figure 14 (Color online) Schematic of spontaneous growth of uncapped Te NPs in various solvents. Reprinted from permission from ref. [41]. Copyright 2016 Nature Publishing Group.

stability of NPs with lower value of zeta potential (−9.7 mV in H_2O, −16.2 mV in CH_3OH, −37.9 mV in CH_3COCH_3, −54.8 mV in CH_3CH_2OH) results in slow growth kinetics because of the higher electrostatic repulsion between them. Hence, it can be summarized that LAL first gives birth to the formation of tiny Te NPs, which rapidly crystallize and attach with each other into Te nanochains, after which period the chains slowly aggregate or self-assembly into agglomerates. Finally these agglomerates undergo extremely slow crystallization and Ostwald ripening to become (sub)microspheres. The reason for the final transformation of all nanotrains and nanocubes towards (sub)microspheres should be due to the lowest surface energy of spheres as compared to other shapes. But why particle chains in CH_2Cl_2 change into cubic is still unknown. This work is of great significance for displaying the overview of the particle growth and demonstrates the possibility to obtain intermediate nanochains by aging the LAL-colloids.

3.2 Nanofiber and nanosheet

While ablating Mn targets in water-containing solutions, besides the NPs, nanofibers and nanosheets are often observed [120]. The difference in the surface energy of the assembled crystals in different directions may result in the anisotropic growth of nanofibers in a template-free colloidal system. But no work has been implemented to verify this speculation for the LAL-synthesized fibers and nanosheets. Some hints can be gained from a recent report by Zhang et al. [30] who characterized both Mn_3O_4 nanosheets and nanofibers obtained by laser ablation of a $Fe_{50}Mn_{50}$ alloy target in water-ethanol mixture liquids with different volume ratios. The Mn_3O_4 nanosheets and nanofibers interestingly share the same phase (ICSD No. 31094) (Figure 15(c) and (d)) and meanwhile a scenario at which time the nanosheets are splitting into nanofibers is captured (Figure 15(a) and (b)). Meanwhile, they also found that in less LAL-induced oxidative environment (lower water ratio in water-ethanol mixtures), the density of nanosheets is larger. All these findings indicate that the nanofibers originate from the nanosheets whose split leads to the formation of nanofibers. A question still exists regarding why the particles attach and evolve into anisotropic nanostructures rather than spherical particles, which are the most often observed particle shape by LAL [60,65]. To further clarify whether Fe species contribute to the formation of such MnO_x nanosheets and nanofibers, the authors did a comparative study by LAL of a pure Mn target in the same solutions and only found 20-30 nm Mn_3O_4 nanocubes made of tiny particles with the size of 8-11 nm [30]. Hence, the presence of Fe atoms or ions for the formation of anisotropic growth of MnO_x nanostructures is confirmed, similar to the auxiliary effect of Fe^{3+} ions for the growth of MnO_2 nano-columns [121]. Hence, besides the reaction-induced growth of the alloy particles as discussed in sect. 2.6, the ions originating from the ionization of the target materials may also dominate the growth of nanostructures as the dopants. This work may inspire more works to be implemented by designing an experiment with different ion additives or solid elements in the alloyed targets that may cause anisotropic growth of the nanomaterials during and after LAL.

3.3 Nanoflower and nanoleaf

Besides the nanostructures shown above, many other kinds

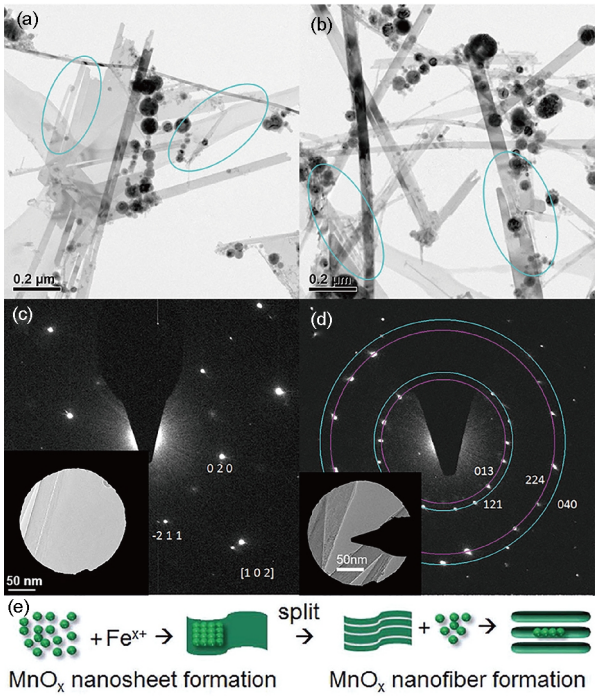

Figure 15 (Color online) Self-split phenomenon. (a) and (b) TEM images showing the split moment of Mn_3O_4 nanosheets towards nanofibers; (c) and (d) SAED of nanosheets and nanofibers; (e) schematic of nanosheet formation in presence of Fe ions and subsequent nanosheet split. Both nanosheets and nanofibers are obtained by LAL of a FeMn alloy target in ethanol-water mixture. Adapted from permission of ref. [30]. Copyright 2017 Wiley-VCH.

have also been synthesized by LAL but their formation mechanisms are still missing. For example, Yang et al. [34] found tiny spherical C_3N_4 particles first attached together to form nanospindles (Figure 16(a)), which interconnected to form a "leaflike" network (Figure 16(b)). When the "leaflike" structures were dense enough they eventually assembled into flowerlike structures (Figure 16(c)). Remarkably, this experiment was performed as long as 3-5 h by LAL of a graphite target in a 5 mL solution containing 35% ammonia, in which case the particle concentration is so high to induce three-stage growth. Assemblies of drop shaped ZnO particles into various dendritic leaf-like nanostructures have been presented by Singh's group [122] and they speculated that the electrostatic attraction between the drop shaped ZnO particles leads to their assembly in an ordered manner. Why the particles evolve into drop shaped ZnO particles is still lack of good explanation, which may find answers from the solvent (methanol) used for LAL or the high particle concentration triggered self-assembly behavior (LAL of Zn in 40 mL methanol for 1 h by long-period LAL because similar results have not yet been found for LAL in aqueous solutions [123-127].

4 Conclusions and perspectives

In this review, we have shown six growth routes for the LAL-synthesized highly active ligand-free particles to evolve into a large variety of nanostructures and NPs, including LaMer-like growth, coalescence, Ostwald ripening, particle (oriented) attachment, adsorbate-induced growth and reaction-induced growth. LaMer-like growth curve serves as the foundation to understand the particle growth of other five mechanisms since it correlates the nucleation-growth events with the LAL-generated active particle seeds, where the C_{crit} is the "switch" to initialize the particle growth for each material under different conditions. For LAL, the atom density in the plasma phase and the particle seeds' concentration in the cavitation bubble are the key factors. When reactions take place in the plasma and bubble phases, reaction-induced growth starts and the reactivity of the reactants determines the degree of particle growth. The formation of nanoalloys [30] and football-like microspheres [27] follows reaction-induced growth route. When the reactions are not possible, extra ions or surfactant additives may adsorb on the seeds' surface to change the surface chemistry of the NPs, especially the surface energy may be altered by the adsorbates, thus influencing the growth trend in different directions. That is why anisotropic nanostructures are often

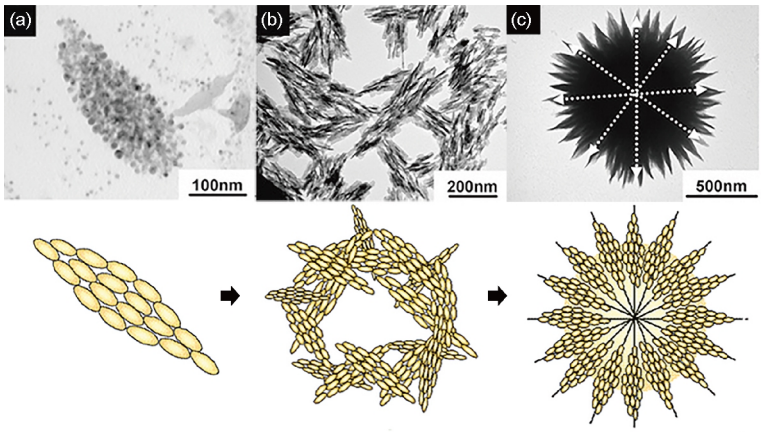

Figure 16 (Color online) (a)-(c) Self-assembly of C_3N_4 NPs into nanospindles and further into nanoflowers. Adapted from permission of ref. [34]. Copyright 2006 American Chemical Society.

found in presence of ions and surfactant additives [30,108,128]. Selective particle attachment on certain facet of the nanostructures controlled by the adsorbate governs the anisotropic growth, as confirmed by Zhang et al. [30], in which case the continuous crystallographic alignment in certain direction may happen following oriented attachment mechanism. For partial crystalline NPs and amorphous NPs, particle attachment followed by recrystallization of the attached NPs leads to the formation of crystalline crystals. Coalescence is similar to the particle attachment mechanism and the only difference is no preferable attachment of particles for the coalescence process [20]. Random particle aggregation is an indispensable step, with the aid of laser sintering, often leading to the formation of polycrystalline particles with stacking faults and grain boundaries, especially apparent for the LAL-synthesized nanoalloys [60,61]. Sometimes, these particle aggregation may gradually undergo a grain growth and causes the change of particle phase overtime [65]. When big particles form through coalescence growth, there exists a difference in particle size and the concentration gradient, which is a favorable condition to trigger Ostwald ripening if the tiny particles are soluble in the bigger ones. That is why coalescence and Ostwald ripening concurrently occur to the Pt NPs as shown by the Barcikowski's group [74]. These six growth mechanisms are not independent but synergetically affect the growth of the LAL-generated particles. However, in which case and to which degree one mechanism dominates a part of or the whole plasma-bubble-liquid phases is still unknown, more systematic investigations are needed.

As deduced from the representative nanostructures mentioned above, some unique features for LAL synthesis technique have turned out: (1) the ability of particle concentration control to trigger particle nucleation-growth. For LAL, it allows both short-period LAL and long-period LAL, enabling the particle concentration constant and shortly above the C_{crit}, that is why unusual nanostructures (e.g., large hollow Mn_3O_4 assembled by cubic units [30], flower-like C_3N_4 made of nanospindles [34] and leaf-like ZnO [122]) and normal spherical particles are both achievable. In particular, long-period LAL with the advantage of producing supersaturated colloids is very appealing for the resultant self-assembly of the colloids, from which route more interesting nanostructures are anticipatable. (2) Reaction-induced growth resulting from the atomization and ionization of the target materials and the liquid molecules, which is the impetus of rapid advance in adopting LAL for alloy [117] or doped [129] or core-shell [30,130] nanomaterial synthesis. (3) Developing high-pressure phase nanomaterials. Since amorphization is a ubiquitous phenomenon during LAL and in some cases amorphous nanomaterials are the intermediate state for high-pressure evolution [66], aging the colloids may help researchers obtain high pressure phase NPs conveniently as demonstrated by Liang's group [65]. It is because of these different features only belonging to LAL that make the synthesized nanostructures meaningful and easily distinguishable from those nanomaterials obtained by other techniques. As the LAL-synthesized ligand-free nanomaterials become increasingly popular for various applications [14], the demand for better control of the nanomaterials as well as the anticipation for novel nanomaterial development will push this field forward steadily.

However, as seen, since the very complex processes for LAL, theoretical work to explicitly explain the particle growth from the thermodynamical and kinetical viewpoints is missing even though progress has been made to clarify how particles form on the basis of molecular dynamics [131]. Moreover, enormous efforts should be devoted to conquering the difficulties in well controlling the LAL processes to unify the formed particles, only in which case the subsequent particle growth can make one achieve desirable uniform products like wet chemical synthesis method. Also, as seen, the growth rates for the most reported nanostructures have not been quantified yet, which is a factor of great significance to control the morphology of the products. Elucidating their correlation with the particle and solution properties, such as thermal conductivity, solubility and liquid viscosity is especially needed. Studies on facet-engineering and interface control are still lacking. Considering the large potential of the well-controlled facet-controlled growth for catalysis, plasmonics and surface-enhanced Raman spectroscopy (SERS) applications [92], this field should deserve more attention for LAL-participating scientists.

This work was supported by the National Key Basic Research Program of China (Grant No. 2014CB931704), the National Natural Science Foundation of China (Grant No. 11304315, 51401206, 11404338, 51371166, 51571186, and 11504375), and the Chinese Academy of Sciences/State Administration of Foreign Experts Affairs (CAS/SAFEA) International Partnership Program for Creative Research Teams.

1 Z. Ge, and S. Liu, Chem. Soc. Rev. **42**, 7289 (2013).
2 J. Lee, S. Mahendra, and P. J. J. Alvarez, ACS Nano. **4**, 3580 (2010).
3 M. Zhu, and C. Yang, Chem. Soc. Rev. **42**, 4963 (2013).
4 C. Zhu, D. Du, A. Eychmüller, and Y. Lin, Chem. Rev. **115**, 8896 (2015).
5 J. Schneider, M. Matsuoka, M. Takeuchi, J. Zhang, Y. Horiuchi, M. Anpo, and D. W. Bahnemann, Chem. Rev. **114**, 9919 (2014).
6 H. Zeng, X. W. Du, S. C. Singh, S. A. Kulinich, S. Yang, J. He, and W. Cai, Adv. Funct. Mater. **22**, 1333 (2012).
7 G. Yang, Prog. Mater. Sci. **52**, 648 (2007).
8 V. Amendola, and M. Meneghetti, Phys. Chem. Chem. Phys. **15**, 3027 (2013).
9 R. Zhou, and F. Li, Opto-Elec. Eng. **44**, 172 (2017).
10 R. Zhou, F. P. Li, and M. H. Hong, Sci. Sin-Phys. Mech. Astron. **47**, 024201 (2017).
11 D. Zhang, and B. Gökce, Appl. Surf. Sci. **392**, 991 (2017).
12 D. Zhang, and S. Barcikowski, *Encyclopedia of Polymeric Nanomaterials* (Springer, Berlin, Heidelberg, 2015), p. 2131.

13 S. Barcikowski, V. Amendola, G. Marzun, C. Rehbock, S. Reichenberger, D. Zhang, and B. Gökce, *Handbook of Laser Synthesis of Colloids* (DuEPublico, Essen, 2016).
14 D. Zhang, B. Gökce, and S. Barcikowski, Chem. Rev. **117**, 3990 (2017).
15 J. Zhang, M. Chaker, and D. Ma, J. Colloid Interf. Sci. **489**, 138 (2017).
16 R. Intartaglia, G. Das, K. Bagga, A. Gopalakrishnan, A. Genovese, M. Povia, E. Di Fabrizio, R. Cingolani, A. Diaspro, and F. Brandi, Phys. Chem. Chem. Phys. **15**, 3075 (2013).
17 V. Amendola, L. Litti, and M. Meneghetti, Anal. Chem. **85**, 11747 (2013).
18 C. Streich, S. Koenen, M. Lelle, K. Peneva, and S. Barcikowski, Appl. Surf. Sci. **348**, 92 (2015).
19 Y. Xia, Y. Xiong, B. Lim, and S. E. Skrabalak, Angew. Chem. Int. Ed. **48**, 60 (2009).
20 N. T. K. Thanh, N. Maclean, and S. Mahiddine, Chem. Rev. **114**, 7610 (2014).
21 V. K. LaMer, and R. H. Dinegar, J. Am. Chem. Soc. **72**, 4847 (1950).
22 V. K. L. Mer, Ind. Eng. Chem. **44**, 1270 (1952).
23 A. Schwenke, P. Wagener, S. Nolte, and S. Barcikowski, Appl. Phys. A **104**, 77 (2011).
24 A. Baladi, and R. Sarraf Mamoory, Appl. Surf. Sci. **256**, 7559 (2010).
25 Z. Du, L. Chen, T. S. Kao, M. Wu, and M. Hong, Beilstein J. Nanotechnol. **6**, 1199 (2015).
26 R. Streubel, S. Barcikowski, and B. Gökce, Opt. Lett. **41**, 1486 (2016).
27 D. Zhang, B. Gökce, C. Notthoff, and S. Barcikowski, Sci. Rep. **5**, 13661 (2015).
28 M. Dell'Aglio, R. Gaudiuso, O. De Pascale, and A. De Giacomo, Appl. Surf. Sci. **348**, 4 (2015).
29 J. Lam, D. Amans, F. Chaput, M. Diouf, G. Ledoux, N. Mary, K. Masenelli-Varlot, V. Motto-Ros, and C. Dujardin, Phys. Chem. Chem. Phys. **16**, 963 (2014).
30 D. Zhang, Z. Ma, M. Spasova, A. E. Yelsukova, S. Lu, M. Farle, U. Wiedwald, and B. Gökce, Part. Part. Syst. Charact. **34**, 1600225 (2017).
31 H. Zhang, C. Liang, J. Liu, Z. Tian, and G. Shao, Carbon **55**, 108 (2013).
32 H. Zhang, J. Liu, Z. Tian, Y. Ye, Y. Cai, C. Liang, and K. Terabe, Carbon **100**, 590 (2016).
33 M. Nath, C. N. R. Rao, R. Popovitz-Biro, A. Albu-Yaron, and R. Tenne, Chem. Mater. **16**, 2238 (2004).
34 L. Yang, P. W. May, L. Yin, R. Brown, and T. B. Scott, Chem. Mater. **18**, 5058 (2006).
35 C. Liang, T. Sasaki, Y. Shimizu, and N. Koshizaki, Chem. Phys. Lett. **389**, 58 (2004).
36 C. X. Wang, P. Liu, H. Cui, and G. W. Yang, Appl. Phys. Lett. **87**, 201913 (2005).
37 T. Sakka, S. Iwanaga, Y. H. Ogata, A. Matsunawa, and T. Takemoto, J. Chem. Phys. **112**, 8645 (2000).
38 S. Ibrahimkutty, P. Wagener, A. Menzel, A. Plech, and S. Barcikowski, Appl. Phys. Lett. **101**, 103104 (2012).
39 S. Ibrahimkutty, P. Wagener, T. dos Santos Rolo, D. Karpov, A. Menzel, T. Baumbach, S. Barcikowski, and A. Plech, Sci. Rep. **5**, 16313 (2015).
40 P. Wagener, S. Ibrahimkutty, A. Menzel, A. Plech, and S. Barcikowski, Phys. Chem. Chem. Phys. **15**, 3068 (2013).
41 J. Liu, C. Liang, X. Zhu, Y. Lin, H. Zhang, and S. Wu, Sci. Rep. **6**, 32631 (2016).
42 N. Bärsch, J. Jakobi, S. Weiler, and S. Barcikowski, Nanotechnology **20**, 445603 (2009).
43 A. Abdolvand, S. Z. Khan, Y. Yuan, P. L. Crouse, M. J. J. Schmidt, M. Sharp, Z. Liu, and L. Li, Appl. Phys. A **91**, 365 (2008).
44 G. X. Chen, M. H. Hong, T. C. Chong, H. I. Elim, G. H. Ma, and W. Ji, J. Appl. Phys. **95**, 1455 (2004).
45 Z. Yan, R. Bao, Y. Huang, A. N. Caruso, S. B. Qadri, C. Z. Dinu, and D. B. Chrisey, J. Phys. Chem. C **114**, 3869 (2010).
46 Y. Xin, K. Nishio, and K. Saitow, Appl. Phys. Lett. **106**, 201102 (2015).
47 H. Wang, and R. H. Davis, J. Colloid Interf. Sci. **159**, 108 (1993).
48 R. M. Mazo, J. Stat. Phys. **1**, 89 (1969).
49 C. A. Schaumberg, M. Wollgarten, and K. Rademann, J. Phys. Chem. A **118**, 8329 (2014).
50 P. Boyer, and M. Meunier, J. Phys. Chem. C **116**, 8014 (2012).
51 V. Svrcek, T. Sasaki, Y. Shimizu, and N. Koshizaki, J. Laser Micro/Nanoeng. **2**, 15 (2007).
52 D. Zhang, M. Lau, S. Lu, S. Barcikowski, and B. Gökce, Sci. Rep. **7**, 40355 (2017).
53 H. Wang, N. Koshizaki, L. Li, L. Jia, K. Kawaguchi, X. Li, A. Pyatenko, Z. Swiatkowska-Warkocka, Y. Bando, and D. Golberg, Adv. Mater. **23**, 1865 (2011).
54 N. Takada, T. Sasaki, and K. Sasaki, Appl. Phys. A **93**, 833 (2008).
55 S. I. Dolgaev, A. V. Simakin, V. V. Voronov, G. A. Shafeev, and F. Bozon-Verduraz, Appl. Surf. Sci. **186**, 546 (2002).
56 C. N. Huang, J. S. Bow, Y. Zheng, S. Y. Chen, N. J. Ho, and P. Shen, Nanoscale Res. Lett. **5**, 972 (2010).
57 E. C. Chang, B. C. Lin, P. Shen, and S. Y. Chen, J. Nanosci. Nanotech. **12**, 8337 (2012).
58 Y. T. Chan, C. H. Wu, P. Shen, and S. Y. Chen, Appl. Phys. A **116**, 1065 (2014).
59 B. Y. Chen, S. S. Lin, P. Shen, and S. Y. Chen, CrystEngComm **17**, 8307 (2015).
60 K. D. Malviya, and K. Chattopadhyay, J. Phys. Chem. C **118**, 13228 (2014).
61 K. D. Malviya, and K. Chattopadhyay, J. Phys. Chem. C **120**, 27699 (2016).
62 D. Liu, C. Li, F. Zhou, T. Zhang, H. Zhang, X. Li, G. Duan, W. Cai, and Y. Li, Sci. Rep. **5**, 7686 (2015).
63 L. Vitos, A. V. Ruban, H. L. Skriver, and J. Kollár, Surf. Sci. **411**, 186 (1998).
64 P. Wagener, J. Jakobi, C. Rehbock, V. S. K. Chakravadhanula, C. Thede, U. Wiedwald, M. Bartsch, L. Kienle, and S. Barcikowski, Sci. Rep. **6**, 23352 (2016).
65 J. Liu, C. Liang, Z. Tian, S. Zhang, and G. Shao, Sci. Rep. **3**, 1741 (2013).
66 T. Ikeya, and M. Senna, J. Non-Crystal. Solid. **105**, 243 (1988).
67 J. Y. Liang, C. H. Wu, Y. Zheng, P. Shen, and S. Y. Chen, Appl. Phys. A **115**, 1429 (2014).
68 Z. Yan, R. Bao, Y. Huang, and D. B. Chrisey, J. Phys. Chem. C **114**, 11370 (2010).
69 M. Zimbone, G. Cacciato, M. A. Buccheri, R. Sanz, N. Piluso, R. Reitano, F. La Via, M. G. Grimaldi, and V. Privitera, Mater. Sci. Semiconduct. Proc. **42**, 28 (2016).
70 P. W. Voorhees, J. Stat. Phys. **38**, 231 (1985).
71 I. M. Lifshitz, and V. V. Slyozov, J. Phys. Chem. Solids **19**, 35 (1961).
72 C. Wagner, Zeitsch. Elektrochem. **65**, 581 (1961).
73 B. L. Cushing, V. L. Kolesnichenko, and C. J. O'Connor, Chem. Rev. **104**, 3893 (2004).
74 S. Jendrzej, B. Gökce, V. Amendola, and S. Barcikowski, J. Colloid Interf. Sci. **463**, 299 (2016).
75 C. Ribeiro, E. J. H. Lee, E. Longo, and E. R. Leite, ChemPhysChem **6**, 690 (2005).
76 A. Poletti, G. Fracasso, G. Conti, R. Pilot, and V. Amendola, Nanoscale **7**, 13702 (2015).
77 O. R. Musaev, A. E. Midgley, J. M. Wrobel, J. Yan, and M. B. Kruger, J. Appl. Phys. **106**, 054306 (2009).
78 J. J. De Yoreo, P. U. P. A. Gilbert, N. A. J. M. Sommerdijk, R. L. Penn, S. Whitelam, D. Joester, H. Zhang, J. D. Rimer, A. Navrotsky, J. F. Banfield, A. F. Wallace, F. M. Michel, F. C. Meldrum, H. Cölfen, and P. M. Dove, Science **349**, aaa6760 (2015).
79 W. Lv, W. He, X. Wang, Y. Niu, H. Cao, J. H. Dickerson, and Z. Wang,

Nanoscale **6**, 2531 (2014).
80 A. Fojtik and A. Henglein, Ber. Bunsenges. Phys. Chem. 97, 252 (1993).
81 A. Henglein, J. Phys. Chem. **97**, 5457 (1993).
82 C. H. Wu, S. Y. Chen, and P. Shen, CrystEngComm **16**, 1459 (2014).
83 S. J. Hsu, S. S. Lin, Y. Zheng, P. Shen, and S. Y. Chen, Appl. Phys. A **122**, 358 (2016).
84 H. Wang, O. Odawara, and H. Wada, Sci. Rep. **6**, 20507 (2016).
85 X. Z. Lin, P. Liu, J. M. Yu, and G. W. Yang, J. Phys. Chem. C **113**, 17543 (2009).
86 E. Giorgetti, M. Muniz-Miranda, P. Marsili, D. Scarpellini, and F. Giammanco, J. Nanopart. Res. **14**, 648 (2012).
87 H. Tabata, M. Fujii, and S. Hayashi, Carbon **44**, 522 (2006).
88 J. Wang, and A. S. Wexler, Geophys. Res. Lett. **40**, 2834 (2013).
89 W. He, CrystEngComm **16**, 1439 (2014).
90 N. Haram, and N. Ahmad, J. Clust. Sci. **26**, 713 (2015).
91 R. Lachaine, É. Boulais, and M. Meunier, ACS Photon. **1**, 331 (2014).
92 A. R. Tao, S. Habas, and P. Yang, Small **4**, 310 (2008).
93 S. Hebié, Y. Holade, K. Maximova, M. Sentis, P. Delaporte, K. B. Kokoh, T. W. Napporn, and A. V. Kabashin, ACS Catal. **5**, 6489 (2015).
94 C. Rehbock, V. Merk, L. Gamrad, R. Streubel, and S. Barcikowski, Phys. Chem. Chem. Phys. **15**, 3057 (2013).
95 M. Wang, Z. Wu, Z. Chu, J. Yang, and C. Yao, Chem. Asian J. **9**, 1006 (2014).
96 A. Menéndez-Manjón, A. Schwenke, T. Steinke, M. Meyer, U. Giese, P. Wagener, and S. Barcikowski, Appl. Phys. A **110**, 343 (2013).
97 L. Kőrösi, M. Rodio, D. Dömötör, T. Kovács, S. Papp, A. Diaspro, R. Intartaglia, and S. Beke, J. Chem. **2016**, 1 (2016).
98 M. Rodio, R. Brescia, A. Diaspro, and R. Intartaglia, J. Colloid Interf. Sci. **465**, 242 (2016).
99 S. D. Angelov, S. Koenen, J. Jakobi, H. E. Heissler, M. Alam, K. Schwabe, S. Barcikowski, and J. K. Krauss, J Nanobiotechnol. **14**, 3 (2016).
100 M. A. Sobhan, M. J. Withford, and E. M. Goldys, Langmuir **26**, 3156 (2010).
101 A. Essaidi, M. Chakif, B. Schöps, A. Aumman, S. Xiao, C. Esen, and A. Ostendorf, J. Laser Micro/Nanoeng. **8**, 131 (2013).
102 M. I. Mendivil, B. Krishnan, F. A. Sanchez, S. Martinez, J. A. Aguilar-Martinez, G. A. Castillo, D. I. Garcia-Gutierrez, and S. Shaji, Appl. Phys. A **110**, 809 (2013).
103 S. Lee, J. H. Shin, and M. Y. Choi, J. Nanopart. Res. **15**, 1473 (2013).
104 K. Yamada, Y. Tokumoto, T. Nagata, and F. Mafuné, J. Phys. Chem. B **110**, 11751 (2006).
105 Y. Y. Fong, J. R. Gascooke, B. R. Visser, H. H. Harris, B. C. C. Cowie, L. Thomsen, G. F. Metha, and M. A. Buntine, Langmuir **29**, 12452 (2013).
106 C. He, T. Sasaki, Y. Shimizu, and N. Koshizaki, Appl. Surf. Sci. **254**, 2196 (2008).
107 C. C. Huang, C. S. Yeh, and C. J. Ho, J. Phys. Chem. B **108**, 4940 (2004).
108 C. Liang, Y. Shimizu, M. Masuda, T. Sasaki, and N. Koshizaki, Chem. Mater. **16**, 963 (2004).
109 T. I. Borodina, G. E. Val'yano, O. A. Gololobova, V. T. Karpukhin, M. M. Malikov, and D. A. Strikanov, Quantum Electron. **43**, 563 (2013).
110 C. Pfeiffer, C. Rehbock, D. Hühn, C. Carrillo-Carrion, D. J. De Aberasturi, V. Merk, S. Barcikowski, and W. J. Parak, J. R. Soc. Interf. **11**, 20130931 (2014).
111 A. Letzel, B. Gökce, P. Wagener, S. Ibrahimkutty, A. Menzel, A. Plech, and S. Barcikowski, J. Phys. Chem. C **121**, 5356 (2017).
112 H. Kwon, K. K. Kim, J. K. Song, and S. M. Park, Bull. Korean Chem. Soc. **35**, 865 (2014).
113 O. M. Magnussen, Chem. Rev. **102**, 679 (2002).
114 S. Z. Khan, Y. Yuan, A. Abdolvand, M. Schmidt, P. Crouse, L. Li, Z. Liu, M. Sharp, and K. G. Watkins, J. Nanopart. Res. **11**, 1421 (2009).
115 C. Lemaignan, M. C. Cheynet, and N. Eustathopoulos, J. Cryst. Growth **50**, 720 (1980).
116 E. Jiménez, K. Abderrafi, R. Abargues, J. L. Valdés, and J. P. Martínez-Pastor, Langmuir **26**, 7458 (2010).
117 S. Hu, M. Tian, E. L. Ribeiro, G. Duscher, and D. Mukherjee, J. Power Sources **306**, 413 (2016).
118 H. Park, D. A. Reddy, Y. Kim, S. Lee, R. Ma, M. Lim, and T. K. Kim, Appl. Surf. Sci. **401**, 314 (2017).
119 Y. Jiang, P. Liu, Y. Liang, H. B. Li, and G. W. Yang, Appl. Phys. A **105**, 903 (2011).
120 B. K. Pandey, A. K. Shahi, and R. Gopal, Appl. Surf. Sci. **283**, 430 (2013).
121 Y. Duan, H. Jing, Z. Liu, S. Li, and G. Ma, J. Appl. Phys. **111**, 084109 (2012).
122 S. C. Singh, and R. Gopal, Appl. Surf. Sci. **258**, 2211 (2012).
123 H. Zeng, G. Duan, Y. Li, S. Yang, X. Xu, and W. Cai, Adv. Funct. Mater. **20**, 561 (2010).
124 K. Kawabata, Y. Nanai, S. Kimura, and T. Okuno, Appl. Phys. A **107**, 213 (2012).
125 H. Zeng, W. Cai, B. Cao, J. Hu, Y. Li, and P. Liu, Appl. Phys. Lett. **88**, 181905 (2006).
126 H. Zeng, W. Cai, J. Hu, G. Duan, P. Liu, and Y. Li, Appl. Phys. Lett. **88**, 171910 (2006).
127 E. Fazio, A. M. Mezzasalma, G. Mondio, F. Neri, and R. Saija, Appl. Surf. Sci. **272**, 30 (2013).
128 C. He, T. Sasaki, Y. Zhou, Y. Shimizu, M. Masuda, and N. Koshizaki, Adv. Funct. Mater. **17**, 3554 (2007).
129 H. Zhang, J. Liu, Y. Ye, Z. Tian, and C. Liang, Phys. Chem. Chem. Phys. **15**, 5684 (2013).
130 T. Simao, D. M. Chevrier, J. Jakobi, A. Korinek, G. Goupil, M. Lau, S. Garbarino, P. Zhang, S. Barcikowski, M. A. Fortin, and D. Guay, J. Phys. Chem. C **120**, 22635 (2016).
131 C. Y. Shih, C. Wu, M. V. Shugaev, and L. V. Zhigilei, J. Colloid Interf. Sci. **489**, 3 (2017).